

Deep Reinforcement Learning for Scheduling and Power Allocation in a 5G Urban Mesh

1st Barak Gahtan
Computer Science dept
Technion
Haifa, Israel
barakgahtan@cs.technion.ac.il

2nd Reuven Cohen
Computer Science dept
Technion
Haifa, Israel
rcohen@cs.technion.ac.il

3rd Alex M. Bronstein
Computer Science dept
Technion
Haifa, Israel
bron@cs.technion.ac.il

4th Gil Kedar
Ceragon Ltd.
Israel
gilke@ceragon.com

Abstract—We study the problem of routing and scheduling of real-time flows over a multi-hop millimeter wave (mmWave) mesh. We develop a model-free deep reinforcement learning algorithm that determines which subset of the mmWave links should be activated during each time slot and using what power level. The proposed algorithm, called Adaptive Activator RL (AARL), can handle a variety of network topologies, network loads, and interference models, as well as adapt to different workloads. We demonstrate the operation of AARL on several topologies: a small topology with 10 links, a moderately-sized mesh with 48 links, and a large topology with 96 links. For each topology, the results of AARL are compared to those of a greedy scheduling algorithm. AARL is shown to outperform the greedy algorithm in two aspects. First, its schedule obtains higher goodput. Second, and even more importantly, while the run time of the greedy algorithm renders it impractical for real-time scheduling, the run time of AARL is suitable for meeting the time constraints of typical 5G networks.

I. INTRODUCTION

As mobile traffic increases, mobile networks must become more software-driven, virtualized, flexible, intelligent, and energy-efficient. 5G is the next-generation cellular network technology aiming to meet these requirements. 5G networks have flexible architectures and can support very high user density [1]. To meet the high bandwidth demands, 5G networks use high-frequency mmWave communication ranging between 30 to 300 GHz. Because of the use of such high frequencies, mmWave signals are susceptible to shadowing and exhibit high attenuation; consequently, the scalability of 5G networks is presently a major challenge [2], [3].

Since mmWave signals require line of sight, 5G mmWave access networks in urban areas must use dense placement of base stations (BSs) compared to 3G and 4G networks. The need to connect a large number of BSs to the backbone imposes several significant technological challenges, such as scheduling of data, placements of BSs, etc. The 3GPP standardization body proposes a multi-hop access architecture called Integrated Access and Backhaul (IAB) [4], which aims to address these challenges.

Deep reinforcement learning (DRL) is a promising solution for addressing tough challenges related to network densification in a 5G multihop mmWave backbone [5], such as routing and scheduling. The Open Radio Access Network (ORAN) alliance suggests conducting offline training using a realistic

representation of the actual environment and deploying the learned policy to the open RAN Intelligent Controller (RIC) [5].

This paper considers a multihop mmWave transport wireless mesh, in which data packets are routed from the core network to the users and vice versa, via a multihop mmWave network. In this network, the BSs are used not only for connecting users to the network, but also as part of the multihop mmWave backbone [6].

We propose a model-free DRL algorithm [7], [8] to address the problems of link scheduling and power control in a multihop mmWave backhaul. To the best of our knowledge, this is the first paper to address these problems using DRL. The proposed DRL algorithm does not make prior assumptions on the interdependencies of the different mmWave links. It is trainable for a wide range of topologies and network interference models and is adaptable to a wide range of traffic workloads. The proposed algorithm determines in real-time which BS pairs should activate their connecting mmWave links during each configurable time slot and using what power level.

Figure 1 illustrates a multihop mmWave backhaul with five BSs. It shows the mmWave links selected by the DRL algorithm to be active during two consecutive slots. In slot s , the algorithm activates the links from A to B , D and E ; the link from E to A ; the link from B to C ; and the link from C to B , each with its own power. In slot $s + 1$, the DRL algorithm activates a different set of links, with different transmission powers.

The rest of this paper is organized as follows. Section II discusses the related work. Section III overviews DRL concepts. Section IV introduces the considered network and interference models. Section V presents the AARL algorithm. Section VI outlines a greedy algorithm that is subsequently used as a baseline for AARL, in the experimental evaluation reported in Section VII. Finally, Section VIII concludes the paper.

II. RELATED WORK

While many papers have examined how to use machine learning for routing or scheduling in communication networks [9]–[11] only a few papers have explicitly addressed the problem of routing or scheduling in a multihop mmWave

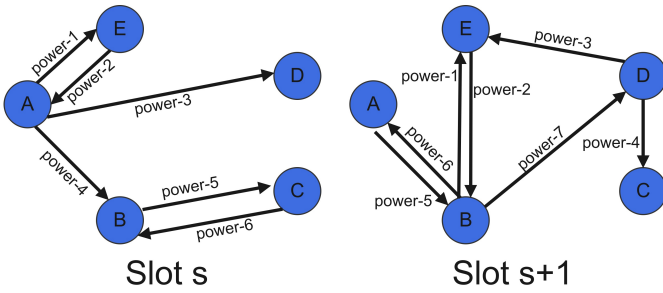


Fig. 1: An illustration of the scheduling decisions made by the proposed algorithm during two consecutive time slots

backbone while taking into account non-trivial interferences [12], [13].

In [14], [15], DRL and gradient decent are used to maximize the throughput of unicast flows in multihop mmWave networks. The authors consider strict per packet deadlines. Their model is different from ours in several aspects: Firstly, they do not consider the interference between links and therefore do not address the problem of power control. Secondly, they assume that a single slot is sufficient for delivering every packet to its final destination, while our paper abandons this unrealistic assumption.

In [16], DRL is used for channel and latency-aware radio resource allocation. This work aims to optimize the uplink scheduling for service-oriented multi-user mmWave RAN in 5G. Multiple application flows are implemented with various statistical models, and the key function modules of the system are designed to reflect the operation and requirements of service-oriented RANs. The characteristics of the mmWave channels utilized in the considered system are collected experimentally and verified via a radio-over-fiber mmWave testbed with dynamic channel variations. In contrast to [16], our work focuses on scheduling in the mmWave backhaul, which is a different problem with different requirements.

In [17], deep deterministic policy gradient (DDPG) is used for radio resource scheduling in a 5G RAN. This work considers multiple users, variable channel conditions, and random traffic arrivals. The limitation of this work is that only Poisson distribution is employed to model the arrival of users. Unlike our work, [17] does not address the backhaul scheduling problem.

In [18], DRL is used for addressing the problem of random blockage of mmWave access links and its effect on the backhaul. The authors learn the blockage pattern and show that the system's dynamics can be captured and predicted, resulting in a better utilization of backhaul resources. While both [18] and our paper use DRL for solving 5G backhaul-related problems, the specific problems addressed by the two papers are substantially different.

In [19], an algorithm called QR-SDN is introduced. QR-SDN is a tabular RL algorithm, which directly represents the routing paths of individual flows in their state-action space. Unlike the present study, the authors do not consider the

interference between the links. Moreover, their algorithm may move a flow from one path to another, while our algorithm sticks to the same path to prevent out-of-order routing.

In [20], a highly effective DRL-based model-free control framework is developed for traffic engineering in a general (not 5G) communication network. The authors consider a general communication network and show how DRL can enable experience-driven networking. The proposed algorithm can be used for learning network dynamics, and for making routing decisions. They use DRL as a model-free routing method, while ignoring interferences.

The present study can also be viewed as an approach to addressing a resource allocation problem using DRL. In this context, [21] previously used DRL for estimating the availability of cache and selecting a proper set of users for interference alignment. In [13], DRL was used for solving the problem of multi-channel access, where every user observes the history of the channel's dynamics and predicts the possible actions of other users. In [22], the authors used DRL for bridging the gap between different performance requirements in a datacenter network. They considered multiple resources, such as bandwidth, cache, and computing.

III. REINFORCEMENT LEARNING

In this section, we provide a brief introduction to DRL. We consider a typical RL setup consisting of an agent interacting with an environment in discrete decision steps. At each decision step t , the agent observes the environment's state s_t , takes an action a_t and, as a consequence receives a reward r_t from the environment. The environment is modeled as a Markov Decision Process, defined as a tuple (S, A, σ, r, S_T) . S and A denote the sets of the environment states and the actions that can be applied by the agent, respectively; $\sigma : S \times A \rightarrow S$ denotes the state transition function, which determines how actions affect the environment state; $r : S \times A \rightarrow \mathbb{R}$ denotes the reward function, which assigns a scalar score (reward) to an action taken by the agent at a given state; and S_T denotes the terminal states that stop the process [23].

The objective of RL is to maximize a cumulative reward by finding the agent's optimal policy [24]–[26]. It seeks to find a balance between acquiring new knowledge (exploration) and using existing knowledge (exploitation) about the environment and the optimal behavior of the agent. A policy is a map $\pi : S \rightarrow A$ that chooses an action $a \in A$ for any given state. A policy may be stochastic, in which case π is interpreted as a conditional distribution $\pi(a|s)$ from which actions are sampled.

Each policy induces a state-action function, also known as the Q-function: $Q_\pi(s, a) = \mathbb{E}_\pi[G_t | S_t = s, A_t = a] = R_s^a + \gamma \sum_{s' \in S} P_{ss'}^a v_\pi(s')$, where R_s^a is the instant reward that can be obtained by taking action a under state s ; $P_{ss'}^a$ is the transition probability from state s to state s' under action a ; γ is the discount factor used to balance the long-term and short-term rewards; and G_t is the cumulative reward from time t , given by $G_t = \sum_{k=0}^{\infty} \gamma^k R_{t+k+1}$. $v_\pi(s) = \mathbb{E}_\pi[G_t | S_t =$

$s] = \sum_{a \in A} \pi(a|s) Q_\pi(s|a)$. This function is essential for determining the optimal policy. In the case of small state-action spaces, the Q-function can be simply computed and tabulated. However, such an approach quickly becomes infeasible as the cardinality of S and A grows. Deep neural networks were shown to be extremely successful in approximating the values of Q with a reasonable number of trainable parameters.

Broadly speaking, there are two approaches to RL problems: model-based and model-free [27]. Model-based learning models the environment and then chooses the optimal policy based on the learned model. In contrast, in model-free learning, the agent establishes the optimal policy through trial and error [27], and the methods are classified into two broad categories: policy optimization techniques and Q-learning value iteration techniques. Q-learning is a model-free RL algorithm that learns the optimal Markov Decision Process policy using Q-values, which estimate the “value” of taking an action at a given state. In policy optimization, the agent directly learns the policy function that maps state to action, without the use of the value function. Among the algorithms that make use of this method is Trust Region Policy Optimization (TRPO) [28]. TRPO is an on-policy method, which means that it attempts to evaluate or improve the policy that is currently being used to take actions, and it uses information gathered from consecutive steps. It is applicable to both discrete and continuous action spaces, and updates policies by taking the most significant possible step to improve performance while maintaining a degree of similarity between the new and old policies. The latter constraint ensures that the new updated policy remains within the trust region of the old policy:

$$\begin{aligned} \max_{\pi'} \mathbb{E}_{\pi'} \left[\frac{\pi'(a|s)}{\pi(a|s)} \hat{A}_\pi(s, a) \right], \\ \text{s.t. } \mathbb{E}_\pi [D_{\text{KL}}(\pi(\cdot|s) | \pi'(\cdot|s))] \leq \delta, \end{aligned} \quad (1)$$

where π' and π denote the new and previous policies, respectively. $\hat{A}_\pi(s, a) \approx Q_\pi(s, a) - v_\pi(s)$ is the approximate advantage function (i.e., the gain in reward relative to the state value when taking a specific action a), D_{KL} denotes the Kullback-Leibler (KL) divergence between two distributions, and δ is a fixed radius. The policy and the advantage functions are practically implemented in DRL settings as neural networks parameterized by some parameter vector θ . Equation 1 can be interpreted as maximizing the objective function that meets the KL constraint term on the policy update step size. The probability ratio between the new policy $\pi_{\theta'}$ and the old one π_θ is defined as $r(\theta') = \frac{\pi_{\theta'}(a|s)}{\pi_\theta(a|s)}$. The objective function maximized by TRPO can be defined as $J_{\text{TRPO}}(\theta') = \mathbb{E} [r(\theta') A_{\theta'}(s, a)]$.

Similarly to TRPO, Proximal Policy Optimization (PPO) [29] is another on-policy algorithm that seeks to improve the policy without risking performance collapse. Moreover, by limiting policy updates at each training step, PPO improves the stability of the agent’s training. PPO is a first-order optimization. In the absence of constraints, the large and small step size updates of the objective function can cause instability or slow convergence. To stay within a small interval around

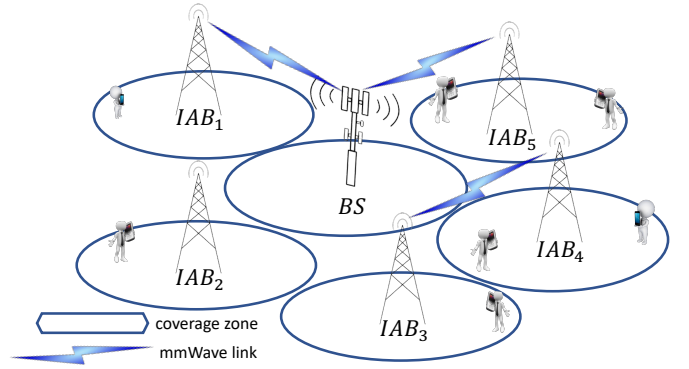


Fig. 2: A multihop mmWave wireless backhaul with five IAB nodes and one BS

1, PPO replaces the complex KL constraint from Eq. 1 with a projection clipping the policy ratio r [29],

$$J_{\text{PPO}}(\theta') = \mathbb{E} [\min\{r(\theta'), 1 + \epsilon\} \hat{A}_\theta(s, a)].$$

The clipping at $1 + \epsilon$ ensures that J_{PPO} lower bounds J_{TRPO} .

IV. NETWORK MODEL AND PROBLEM STATEMENT

A. The Network Model

Following [30]–[34], we consider a multihop mmWave mesh, where data packets are received from the core network and are routed to and from the users via one or more 5G mmWave links. In 5G, two types of mmWave nodes exist, BSs and IABs. The difference between the two is that an IAB is connected to other mmWave nodes, and to some users, while a BS is connected only to other mmWave nodes (see Figure 2). Since this paper focuses on the transition of packets between mmWave nodes, and not between the users and these nodes, we do not distinguish between an IAB and a BS, and refer to both as BSs.

In the considered network model, the RIC receives a demand vector v_i from every BS before the beginning of every time slot. The RIC determines which mmWave links will be established during the next slot, and using what power. Each BS_i has a buffer of waiting packets associated with every neighbor BS_j . This buffer is referred to as $B_{i \rightarrow j}$. If an mmWave link is established from BS_i to BS_j during some slot, this link is used for transmitting packets from $B_{i \rightarrow j}$ to BS_j . The demand vector v_i sent by BS_i to the RIC indicates the number of packets that BS_i needs to transfer to each neighbor BS_j .

Since sending the demand vector from each BS to the RIC takes some non-negligible time, each BS is required to send its demand vectors for slot $s + 1$ at the beginning of slot s . For every neighbor BS_j , this vector indicates the number of packets waiting to be transmitted from BS_i to BS_j at the beginning of slot s . Since the RIC knows which links are activated during slot s , it can estimate the number of packets that BS_i will be able to transmit to every neighbor during

slot s , and therefore the number of waiting packets remaining in the buffer of BS_i will have just before slot $s + 1$ starts. The decision which links to activate during slot $s + 1$ is made by the RIC after it gathers the demand vectors from all BSs. The demand vectors and the controller's scheduling decisions are exchanged over a special control channel, such as 4G-LTE channels [35]–[37], independent of the mmWave infrastructure.

Routing is always made on the shortest paths for the following reasons: (1) to ensure in-order delivery of packets belonging to the same flow; (2) to minimize bandwidth consumption and maximize total throughput; (3) to prevent routing loops without using a complex routing protocol; and (4) to reduce the dimension of the DRL optimization problem.

Suppose that the RIC decides to activate the link from BS_i to BS_j during a specific slot s . This implies that during this slot, packets are transmitted from BS_i to BS_j . These packets are received by BS_j either before or during s . We do not consider a layer-2 flow control protocol due to the negative impact of head-of-the-line blocking on the total throughput. Thus, it is possible that some of the packets sent by BS_i to BS_j do not have an available buffer capacity and are therefore dropped by BS_j .

The most important component of an ML scheduling algorithm is the definition of an appropriate optimization criterion. In our case, the minimization of the average delivery time is not a good choice, as it encourages the algorithm to drop many packets to minimize the delivery time of the delivered packets. Maximizing the total throughput is a better option, but the total throughput depends on the total load, which, in turn, depends on the congestion control protocol. With this protocol, the load increases when the packet loss decreases and vice versa. Thus, we believe that the best criterion to minimize is the total number of dropped packets.

B. The Interference Model

Let l be the mmWave link from BS_i to BS_j . Let the transmission power of BS_i be $P_i(l)$. The received power at BS_j can be calculated according to the Friis transmission equation [38]. The equation defines the free space path loss (FSPL) as a function of the transmit power $P_i(l)$, the received power at BS_j , the distance between the two antennas, and the antennas' gains in a free-space communication link:

$$\text{FSPL}(i,j) = D_T D_R \left(\frac{c}{4\pi D(i,j)f} \right)^2. \quad (2)$$

Here, c denotes the speed of light, $D(i,j)$ is the distance between BS_i and BS_j , D_T and D_R are the directivities of the transmitting and receiving parabolic antennas respectively, and f is the radio carrier frequency. FSPL represents the loss factor depending on the transmit distance and wavelength. According to the radiation pattern function, the received signal D_R is affected by the signal angle of arrival, where θ_R is the deviation of the beam direction from the normal to the receiver

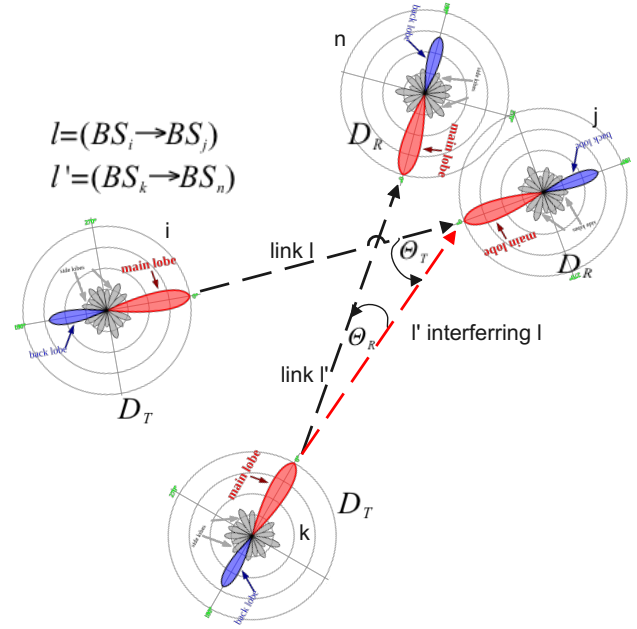


Fig. 3: The interference between two active mmWave links

plane, in the following way: $D_R \propto e^{-\frac{4(\theta_R)^2}{\sqrt{2}}}$. The received power at BS_j is given by,

$$P_{R_j}(l) = P_i(l) - \text{FSPL}(i,j) - \eta,$$

where η is a uniform thermal noise. D_T is defined similarly using the transmit angle θ_T (refer to Fig 3).

Let l' be another link transmitting from BS_k to BS_n at power $P(l')$. This link induces an interference in link l , which is defined as $I(l, l')$. Assuming that all interferences are summed up adversarially, we define the effective receive power of link l as

$$P_{\text{Reff}}(l) = P_R(l) - \sum_{l' \neq l} I(l, l'). \quad (3)$$

Thus, the actual capacity of link l is given by $C(l) = B \cdot \log_2(1 + P_{\text{Reff}}(l))$, where B is the link's nominal bandwidth (in the absence of any interference). The number of bits that can be transmitted over l is given by $N_l = C_l \Delta t$, where Δt is the configurable slot duration. Figure 3 illustrates the interference between links l and link l' . When network interference level reaches 100%, only one link can transmit at a time.

C. Integration into ORAN deployment

The ORAN Alliance proposes an architectural innovation based on two core principles [39]. Firstly, it promotes a model where the BSs are virtualized and divided across multiple network nodes. Secondly, it defines the RAN-RIC, which provides a centralized abstraction of the network, and allows operators to implement and deploy custom control plane functions.

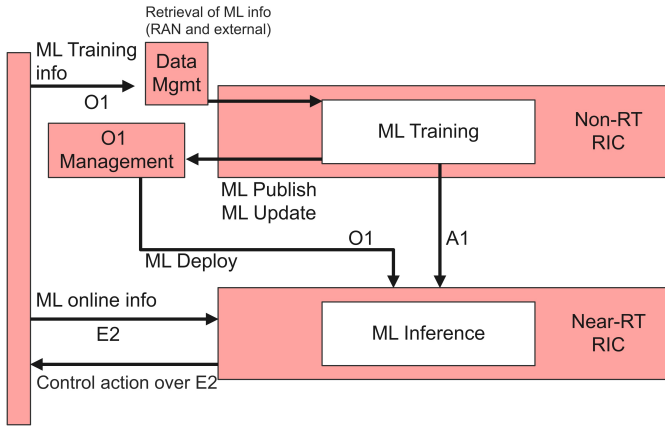


Fig. 4: ORAN deployment scenario [5]

ORAN’s architecture defines three control levels for different timing constraints: real-time (RT), near-real-time (near-RT), and non-real-time (non-RT). RT operations are carried out by the network elements, whereas non-RT and near-RT operations are carried out by the RIC. While the training of an ML algorithm is conducted at the non-RT level, the inference of trained neural network is deployed at the near-RT level, where it interacts with the network elements, receives their measurements, and controls their configurations and policies [40], [41].

Figure 4 illustrates ORAN’s training phase and an inference phase. Specifically, the considered deployment of the proposed algorithm corresponds to scenario 1.2 in Section 4.1 of [42]. During the training phase, the environment provides AARL with the demand vector of the BSs. During the inference phase, the weights of the AARL’s neural network are published to the near-RT RIC via the O1 interface. AARL operates at the near-RT, where it receives the vector demands from all BSs via the E2 interface prior to the beginning of the next time slot and sends the scheduling decision to the BSs via the E2 interface. As stated in Chapter 5 of [42], the near-RT loop must adhere to the time of 10ms time budget.

V. AARL SCHEDULING ALGORITHM

Scheduling is a decision-making activity, which is typically represented and solved as a utility maximization problem. The formulation of the problem is based on a mathematical model, which requires assumptions and approximations. In a 5G scenario, numerous aspects, including the users’ mobility pattern and the traffic model influence the system modeling. These aspects make the multihop mmWave communication network a highly dynamic system. Hence, it is nearly impossible for such a model to account for all these and other factors.

DRL offers an innovative approach to solving decision-making problems in the absence of an explicit mathematical model. A DRL agent approaches the optimal solution of a Markovian Decision Process by learning from its interaction with its environment, and is trained to make decisions that maximize the reward function.

Existing solutions for scheduling and routing usually rely on network information exchange, resulting in a trade-off between overhead and performance. In contrast, DRL seeks to optimize the network tasks through a trial-and-error process that does not require explicit or instantaneous network information. A DRL algorithm can be model-free, which means that it does not require explicit knowledge of the interdependencies between different mmWave links. Therefore, we believe that a DRL-based algorithm is an excellent choice for performing scheduling and power control decisions in a multihop mmWave wireless network.

The environment and agent definitions used by AARL for deciding which mmWave links will be activated during each slot are as follows:

- Training is divided into episodes. Each episode is a sequence of slots required to completely deliver a traffic matrix. A traffic matrix indicates the amount of packets with a source and destination. When an episode starts, the agent is given a traffic matrix and an interference matrix. Each entry in the interference matrix $I_{i,j}$ indicates the amount of interference mmWave link i induces on mmWave link j . Packets that are dropped or successfully delivered are removed from the system. The interference matrix is assumed to be fixed for the entire episode because of episode’s relatively short duration.
- The episode ends when each packet either reaches its destination or is dropped.
- Each slot is a system step. After each step, the agent receives a reward for making good scheduling decisions during that step.
- The agent knows which link each packet should traverse to reach its destination over the shortest path.
- Establishing the interference model and removing or dropping packets from various buffers are executed by the DRL’s environment. The environment validates every decision the agent makes.
- During each step, multiple packets can move between neighboring BSs over activated links. However, each packet can move only one hop per step. This limitation is relevant only to the DRL. During a real-time slot, a packet can be routed multiple times, if the relevant links are activated.
- The maximum capacity of each link is determined by the given topology. Throughout the episode, the interference model affects each step dynamically, by reducing the capacity of each activated link according to its power and the power of the other activated links.

When using an on-policy algorithm such as PPO, the agent learns from consecutive steps by assessing the quality of its decisions using a reward function. Thus, the best policy is learned by taking a small step at a time, while improving the current agent’s policy. The goal of the agent is to find the best strategy suited for the environment. AARL employs a PPO algorithm for finding a good schedule for each step under varying interference and workload distributions. The traffic

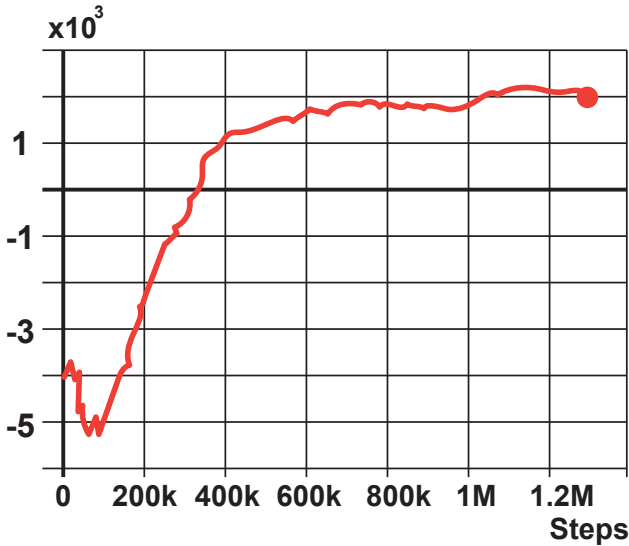


Fig. 5: Example of the convergence of the reward function for the 20-AARL-DS agent

matrix and interference matrix for time step t are used as an input to AARL.

We trained AARL on a variety of traffic and interference matrices to ensure that it will make good decisions also for workloads unseen at training. The training set comprised a uniform workload of packets with varying interference levels. However, as we demonstrate in the evaluation phase, the method performs well also on highly skewed workloads, e.g., when all the packets originate from 10% of the BSs and are destined to 90% of the BSs, or vice versa. Training is conducted over a period of several consecutive episodes. AARL converges the following way: First, AARL converges to a steady reward - each training run of an agent is sampled every 50,000 steps. After sampling, the best checkpoint of weights is taken by looking at the reward's function graph. The higher the plot, while being stable and not over-fitting, the better the checkpoint is. Second, AARL outperforms the greedy algorithm, as shown in Figure 5. When both of the steps are achieved, training is terminated.

The state space of the DRL is concatenated from several vectors. The first part of the state vector indicates the current load on each buffer. The i '-th entry of this vector represents the load fraction for the i '-th buffer of a specific mmWave link. The loads ranges between $[0, 1]$, where 0 indicates an empty buffer and 1 indicates a full one. The second component of the state vector indicates the percentage of packets waiting in each buffer in proportion to all the packets in the system. For instance, if there are 1,000 packets in all the buffers and only 10 in the considered buffer, this entry for the considered buffer is 0.01. The third state vector component is the interference matrix, which is fixed for the entire episode.

The action space contains vectors indicating the power assigned to each mmWave link. Each entry in the action vector corresponds to a specific mmWave link in the topology. Here,

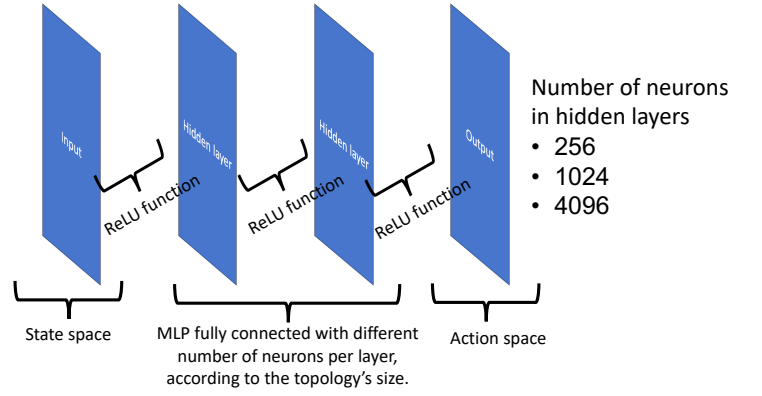


Fig. 6: The neural network used by AARL

0 indicates that the link is not chosen for this step, and 1 indicates that it is chosen to work at maximum power. The greedy algorithm (described in Section VI) uses power steps of 0.1 between 0 and 1, while AARL uses 0.01 steps. Hence, the total number of power levels is 11 for the greedy algorithm and 101 for AARL. This is because the run time of AARL is not affected by the number of power levels, whereas that of the greedy algorithm is dominated by this number.

As shown by Figure 6, the state space is AARL's input, and it is composed of several load vectors from the system. The middle layers are Multi-Layer Perceptron (MLP) fully connected neural networks with a different number of neurons, depending on the size of the topology. The output is the action space, which is the selected set of mmWave links and their selected power level.

Developing a good reward function while promoting the minimization of the number of dropped packets is a major obstacle of an efficient RL-based solution. Assuming that most connections are regulated by a TCP (or TCP-like) congestion control, minimizing the number of lost packets will maximize the total throughput. Our reward function for each step t is therefore:

$$R_t = -\beta - \alpha \frac{D}{P} + \frac{M}{P}, \quad (4)$$

where P is the total number of packets in the system before the step starts (i.e., the traffic load), and D is the total number of packets dropped during the step, assuming that a packet is dropped if it is forwarded to the next hop but cannot be stored there due to buffer overflow. Thus, $\frac{D}{P}$ is the fraction of dropped packets. The reward function should be inversely proportional to it.

We added another component to the reward function to encourage AARL to move as many packets as possible during each step. The total number of packets in-transit during the step is denoted by M . Thus, $\frac{M}{P}$ represents the fraction of moving packets, and the reward is proportional to it. α is a scaling factor that indicates the importance of the first term over the second. Finally, the β term aims to penalize the system for each additional step required to deliver the traffic demand.

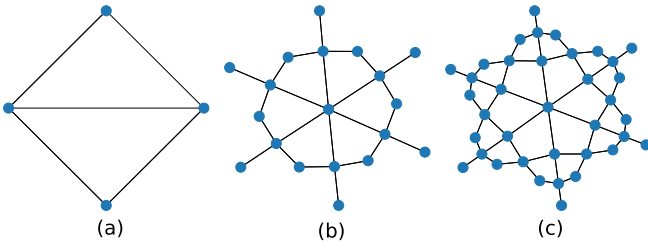


Fig. 7: The three topologies used for AARL's training

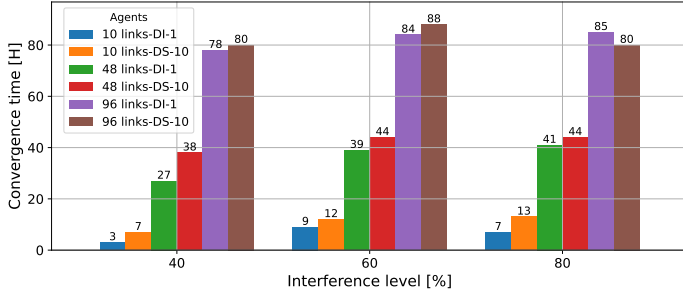


Fig. 8: The convergence time of the various AARL algorithms for different interference levels, with a uniform workload

We trained the system with two α values: 1 and 10, and one β value of 1.

In addition to the chosen reward function, several other reward functions were tested. Their results are not reported in this paper due to their insufficient performance. A reward function that demonstrated performance comparable to the selection function (Equation 4) was $r_t = -p - s_t$. Here, p is the penalizing term as explained before, scaled with three different values $\{-1, -0.1, -10\}$ for each additional step required to deliver the traffic matrix. s_t is the number of steps each packet was delayed relative to the shortest path it should have taken without delay. For instance, if the shortest path for a particular packet to reach its final destination is three hops, and the total number of steps that packet took to reach its destination is five, then the reward function will penalize with two, one for each additional step.

We trained AARL on three topologies provided by Ceragon Ltd. (refer to Figure 7):

- A topology with 4 nodes and 10 links.
- A topology with 19 nodes and 48 links, which represents a medium-size ORAN backhaul network.
- A topology with 37 nodes and 96 links, which represents a large-size ORAN backhaul network.

A unique interference matrix was generated for each episode using the interference model described in Section IV. This allowed us to simulate many interference scenarios, corresponding to different weather and environmental conditions, using the noise term described in the interference model. AARL was trained with data packets that were generated from each BS and with different interference matrix for each episode.

When training starts, the capacity of each mmWave link is sampled from a uniform distribution of $[115, 125]$ packets per time step. Each buffer in the system has a capacity of 650 packets, the size of the buffer can be configurable. AARL is trained using Stable Baselines3 PPO agents [43] in the following way; Five different PPO agents are trained, each with one of the following network interference levels: 20%, 40%, 60%, 80%, and 100%. Recall that when the interference level reaches 100%, only one mmWave link can transmit at full power. During training, the learning rate was set to $3 \cdot 10^{-4}$.

Figure 8 shows the time to convergence of the training phase of the various AARL algorithms for different interference levels. Recall that training is stopped when the reward function converges (see Figure 5), and AARL drops less packets than the greedy algorithm. For example, for a topology with 96 mmWave links, AARL with $\alpha=1$ requires 85 training hours at interference level of 80%. For a topology with 48 mmWave links, AARL with $\alpha=1$ requires 41 hours at the same interference level.

The training time appears to be dominated by the topology size and the network load. As the topology size increases, the state and action spaces increase as well. For example, the action space is a vector of 96-dimensions for the 96-link topology, since it has an entry per each mmWave link. Similarly, for the 48-link topology, the vector has 48 dimensions. The implication on the state space is as follows. For the 48-link topology, the state space has 3 vectors: the first is with 48 entries; the second is also with 48 entries; and the third is with $48 \cdot 48 = 2,304$ dimensions. Therefore, the total dimension of the state space is $48 + 48 + (48 \cdot 48) = 2,400$. In contrast, the 96-link topology has two vectors each with a size of 96 entries, and a vector of $96 \cdot 96 = 9,216$ entries. Therefore, the state space dimension is $96 + 96 + (96 \cdot 96) = 9,408$. When the spaces are larger, the agent needs to learn more complex policies, requiring longer training time.

Additionally, as the level of interference increases, an episode length increases, since fewer mmWave links can transmit during each step. This phenomenon is illustrated by Figure 8. For example, the 10-AARL-DS agent converges after 7 hours for the 40% interference level, after 12 hours for the 60% interference level, and after 13 hours for the 80% interference level. The trend is similar for all other agents.

The length of an episode is another statistic that helps to decide when to stop training. When looking at the collected statistics from the greedy algorithm's runs, we compared the number of steps before completion. The smaller this number, the better the network was utilized, as long as the number of dropped packets does not deviate too far from the greedy algorithm's statistics.

For the small network topology, we used a fully connected MLP neural network with an input size of 120 neurons. The input is made of two load vectors as in the state space, and an interference matrix appended at the end. The size of each load vector is $[1 \times 10]$ and the size of each interference matrix is $[10 \times 10]$. For the MLP, we used two hidden layers of 256 neurons each, with a ReLU activation function between them.

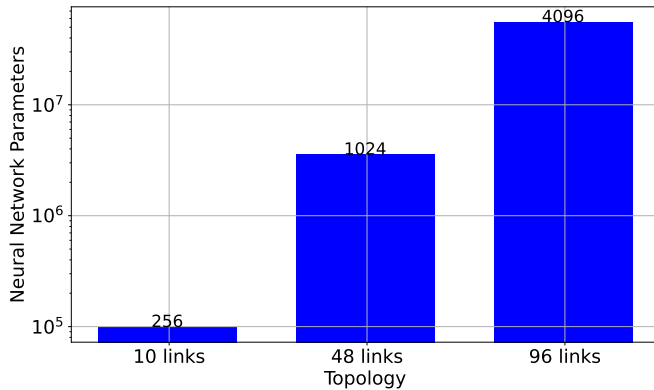


Fig. 9: The number of trainable parameters required to achieve comparable performance for each multihop mmWave network topology (note the logarithmic scale of the vertical axis)

The output layer was the DRL formulation’s action space, which consists of ten links with an output neuron for each mmWave link. There are 99,338 trainable parameters in this network.

For the medium network topology, we used a fully connected MLP neural network with an input size of 2,400 neurons. The input is made of two load vectors of size $[1 \times 48]$, and an interference matrix of size $[48 \times 48]$ appended at the end. For the MLP, we used two hidden layers of 1,024 neurons each, with a ReLU activation function between them. The output layer was the DRL formulation’s action space, which consists of 48 links with an output neuron for each mmWave link. There are 3,557,424 trainable parameters in this network.

Finally, for the large network topology we also used a fully connected MLP with an input size of $[1 \times 96] + [1 \times 96] + [96 \times 96] = 10,308$. Also here, the input is made of two load vectors of size $[1 \times 96]$, and an interference matrix appended at the end. There are two hidden layers in the MLP, each with 4,096 neurons, connected via a ReLU activation function between them. The output layer has 96 neurons, each representing one mmWave link. The number of trainable parameters in this neural network is 55,713,888.

Figure 9 compares between the number of neural network parameters and the number of neurons in the hidden layers for each of the three topologies. We observe that as the number of links in the multihop mmWave topology size increases linearly, the size of the neural network increases exponentially. Appendix A contains additional training statistics. In the future, it may be worthwhile to search for the optimal neural network architecture for each topology. Tailoring a specific neural network for a specific use case can enhance performance [44], [45]. Since we used a simple neural network architecture with two identical hidden layers, designing a better neural network architecture can affect the training time, and enhance the performance of real-time decisions.

Training was performed on a system equipped with AMD Ryzen Threadripper PRO 3955WX 16C CPU 3.9G running at 64MB cache, and 64GB of CRUCIAL CT8G4DFRA32A

RAM clocked at 3200MHz. Program execution was performed solely on the CPU. The CPU-based simulation of the environment, such as moving packets between buffers and calculating the various interference, introduced a CPU-GPU data transfer overhead, negating the advantages of GPU acceleration.

VI. A BASELINE GREEDY ALGORITHM

We now present the greedy algorithm (GREEDY), whose performance was used as a baseline for AARL. The input for GREEDY is a traffic matrix for each BS and an interference matrix. It determines which mmWave links will be activated during the next slot, and what power will be used for each activated link.

GREEDY maintains a set L of all the links considered for the next slot, and a set S of all the links it has already chosen for the next slot. Initially, L contains all the links and S is empty. During each iteration, GREEDY considers one link l , which is randomly chosen from L . Then, it decides whether to add l into S and using what power.

Adding a link l to S has both positive and negative contributions to the network performance. The positive part, termed *capacity gain* (C^+), is due to the fact that packets can be forwarded over this link. The negative part, termed *capacity loss* (C^-), is due to the interference between the new link and previously chosen links. The difference between C^+ and C^- is referred to as the *residual profit* (RP).

The capacity gain of adding l into S using power P_R is given by Eq. 3, which indicates the number of packets to be transmitted over this link during the next slot if it is activated using the considered power. Then, for each link l' previously added into S , GREEDY computes the difference between the new and old effective received power of l' while considering the new link l and its power P_R . The capacity loss is the number of packets that could not be routed in the next slot due to the interference of link l :

$$C^- = \sum_{l' \in S} (P_{\text{R,eff}}(l'_{old}) - P_{\text{R,eff}}(l'_{new})) \frac{C(l')}{P_R(l')}.$$

To summarize, GREEDY chooses a random link l from L , until L is empty and performs the following:

- 1) For each possible power p , it decides what is the RP of adding l with power p .
- 2) If the RP is positive for some p , l is added to S with p for which the RP is maximum. If there is no p for which the RP is positive, l is not into S .
- 3) After a decision is made for l , it is removed from L .

When L is empty, S contains the selected power for the next slot for each mmWave link.

GREEDY’s time complexity is $O(E^3 \cdot \#power\ levels)$, where E is the number of mmWave links in the topology. We implemented GREEDY with eleven distinct power levels: between 0 to 1 with 0.1 steps. It’s given that a typical dense urban network is expected to have at least a few tens of mmWave links, and that a typical slot length is a few ms [46]. GREEDY’s time complexity renders it impractical for deployment.

| Workload | Topology | | |
|-------------|--------------------|---------------------|--------------------|
| | Small (10-link) | Medium (48-link) | Large (96-link) |
| Uniform | 2,304 | 10,812 | 45,246 |
| Few-to-many | 1,800 | 3088 | 57,600 |
| Many-to-few | 1,800 | 13,184 | 57,600 |

TABLE I: Evaluation statistics for each combination of topology and workload

While GREEDY is impractical for real-time networks, we use it as follows: Before AARL’s training begins, we run GREEDY to collect data on the percentage of dropped packets and the average number of slots required to deliver different traffic demand matrices. This information is then used for helping to decide when the training of AARL can be stopped.

VII. EVALUATION

Since no previous paper addresses the mmWave link scheduling and power control problem, we cannot compare our AARL results to previous work. Still, we compare the results of AARL to those obtained by GREEDY, although the time complexity of GREEDY renders it impractical for ORAN.

Throughout this section we consider our three topologies with three different workloads: (a) a uniform workload, where each of the N BSs sends and receives the same amount of data; (b) a few-to-many workload where 10% of the BSs send data to 90% of the BSs; and (c) an incast many-to-few workload where 90% of the BSs send data to 10% of the BSs. We simulated a mmWave backbone according to the 3GPP use cases [47]. The simulation is continuous in the sense that data packets enter the mmWave backbone on a continuous basis, either from the core network or from users via the BSs.

As explained in Section IV, the RIC makes scheduling and power control decisions for slot $s+1$ during slot s . To this end, it receives a vector demand from each BS via the appropriate interface. The vector demand is then corrected by the RIC, to take into account the links that are activated during slot s . The RIC sends its scheduling decision to all BSs via the appropriate interface after deciding which links will be activated during slot s .

The statistics of the system parameters during the evaluation phase are similar to those used during the training phase. The length of each buffer is set to 650 packets, and the maximum capacity of each mmWave link is 120 packets per slot. For the uniform workload and the small topology (10 links), the system starts with 2,304 packets whose sources and destinations are randomly determined using uniform distribution. For the uniform workload and the medium topology (48 links), the system starts with 10,812 packets whose sources and destinations are uniformly distributed. For the uniform workload and large topology (96 links), the system starts with 45,246 packets whose sources and destinations are uniformly distributed. Table I summarizes the above numbers, and also

presents the number for the other two workloads considered in this section: the few-to-many and the many-to-few.

The interference matrix for each topology is calculated at the beginning of the corresponding scenario. Each time, a different interference level is used ranging between 0% and 100%, where 100% means that only one mmWave link can concurrently transmit. Figure 10 compares the performance of two AARL versions to that of GREEDY. These versions are called AARL-DS and AARL-DI. The former has $\alpha=10$ in its reward function, and the latter has $\alpha=1$.

Figure 10 shows the goodput obtained by the various algorithms for different interference levels. The goodput is defined as 100% minus the percentage of lost traffic, and it is normalized to the goodput of GREEDY (i.e., GREEDY’s goodput is considered 100%). We can see in Figure 10(a) that for the 10-link topology the goodput of AARL-DI and AARL-DS is identical to that of GREEDY. Additionally, the interference introduced by a small-scale topology is minor, and there is no packet drop. For the 48-link and 96-link topologies, Figure 10(b) and Figure 10(c) show that AARL-DS is better and AARL-DI is worse than GREEDY. Unlike GREEDY, which only prioritizes moving as many packets as possible within the interference caused by the various mmWave links, AARL-DS is trained to prioritize the throughput, while taking into account the interference between the different mmWave links and the number of dropped packets. Therefore, AARL-DS performs roughly 10% better than GREEDY.

For the additional workloads presented in this section, we consider only AARL-DS and not AARL-DI. Figure 11 shows the goodput obtained by AARL-DS and GREEDY, for the various interference levels on a workload of few-to-many. The trend is similar to the uniform workload for all topologies.

Figure 12 shows the goodput obtained by both algorithms for the many-to-few workload. Figure 12(a) shows that for the 10-link topology, the goodput of AARL-DS is better than GREEDY for the majority of the interference levels. Since it is a small size topology, sending to 10% of the BSs means that only one BS is a destination. This can result in a high packet loss. However, because AARL-DS is capable of intelligently scheduling mmWave links to maximize throughput while dropping a lower number of packets, it performs better. For the 48-link and 96-link topologies, Figure 12(b) and Figure 12(c) show that the trend is similar to what we saw in Figure 10 and Figure 11.

The most important advantage of AARL compared to GREEDY is its execution time, as shown in Figure 13 on a logarithmic scale. As discussed in Section IV, AARL has to meet the time constraints of the slot duration, which is at least 10 ms. It is evident that the running time of GREEDY is between 1 and 2 orders of magnitude larger than that of AARL, making it infeasible for real deployment. It is also evident that GREEDY is much more affected by an increase of the topology. We can also see that AARL is capable of meeting the time constraint of around 10 ms. Table II summarizes the running times of both algorithms for each topology and workload.

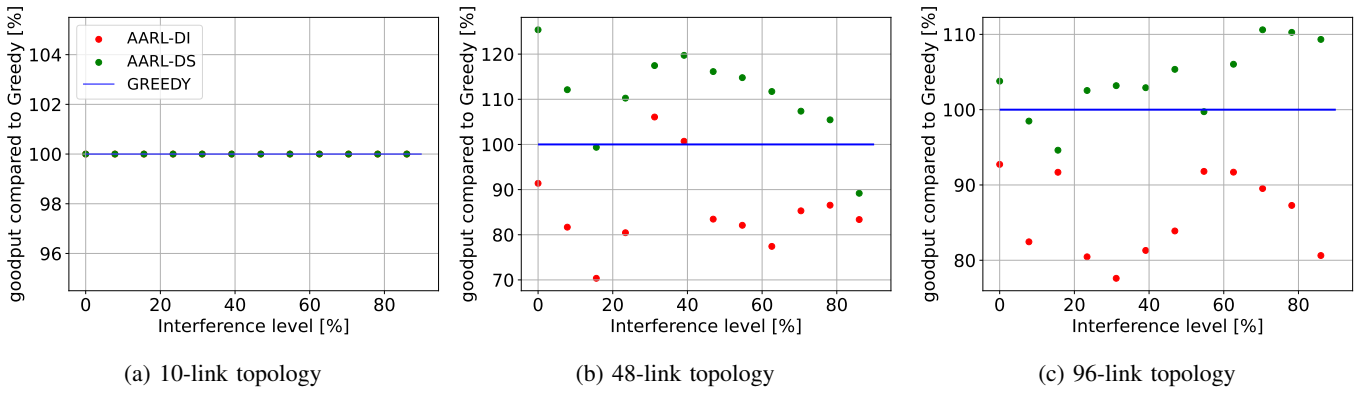


Fig. 10: The performance of AARL vs. GREEDY for the uniform workload (GREEDY/RL)

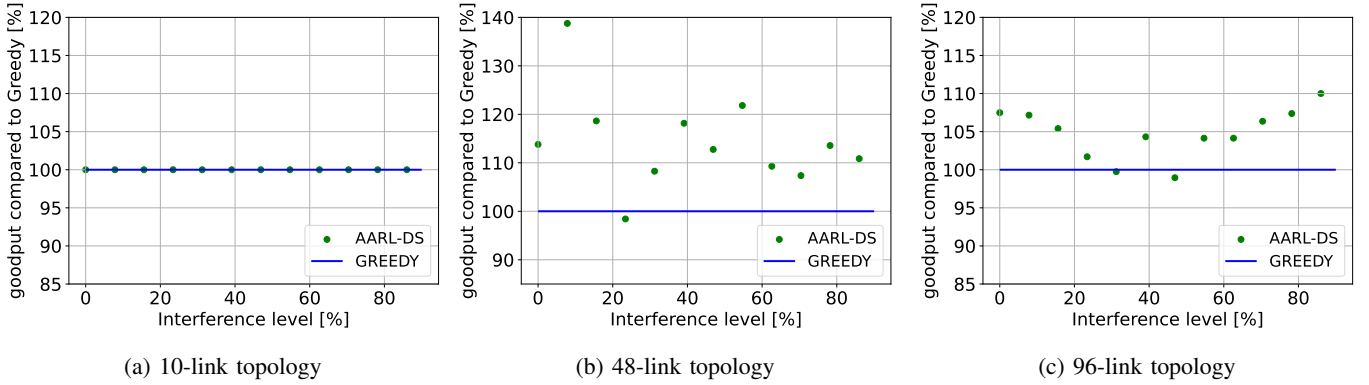


Fig. 11: The performance of AARL vs. GREEDY for the few-to-many workload (GREEDY/RL)

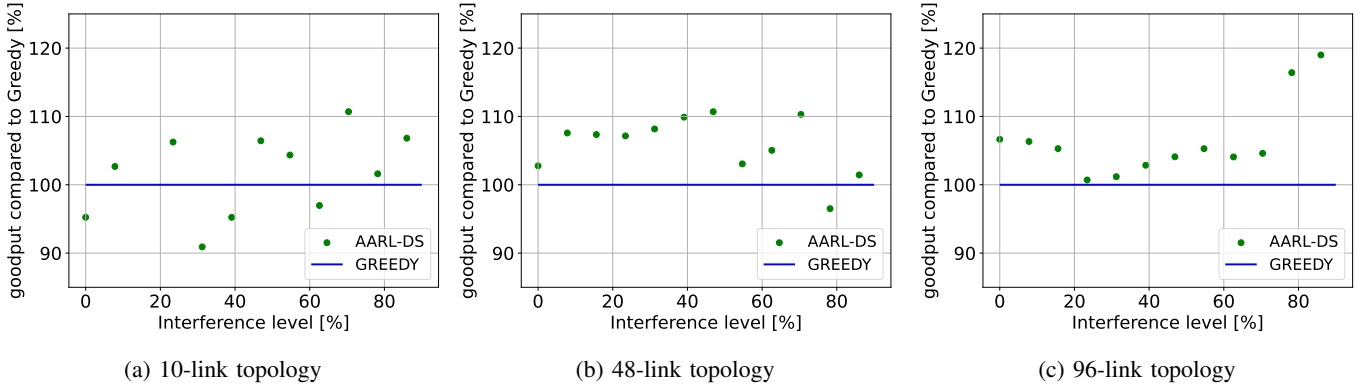


Fig. 12: The performance of AARL vs. GREEDY for the many-to-few workload (GREEDY/RL)

Figure 13 summarizes the time it takes for GREEDY and AARL to make a scheduling decision for the various topologies and workloads. Despite the fact that AARL employs a larger neural network with more trainable parameters when the topology increases, its running time is independent of the topology size. In contrast, the running time of GREEDY strongly depends on the topology size. We can also see that the workload type does not affect the running time of AARL, but it does affect the running time of GREEDY.

The hardware used in the evaluation is the same as used for the training. Since the program is not optimized for GPU

execution, as explained in Section V, we can assume that AARL will make scheduling decisions faster in a real system that will use GPUs, while GREEDY will not. This is because matrix calculations performed on GPUs are much faster than on CPUs. In our case, it took about 10 ms for AARL to calculate a scheduling decision for each slot of the 96-link topology, which is a typical topology in 5G networks [46].

VIII. CONCLUSIONS

We studied the problem of scheduling real-time flows over a multihop mmWave wireless mesh. We developed a model-free

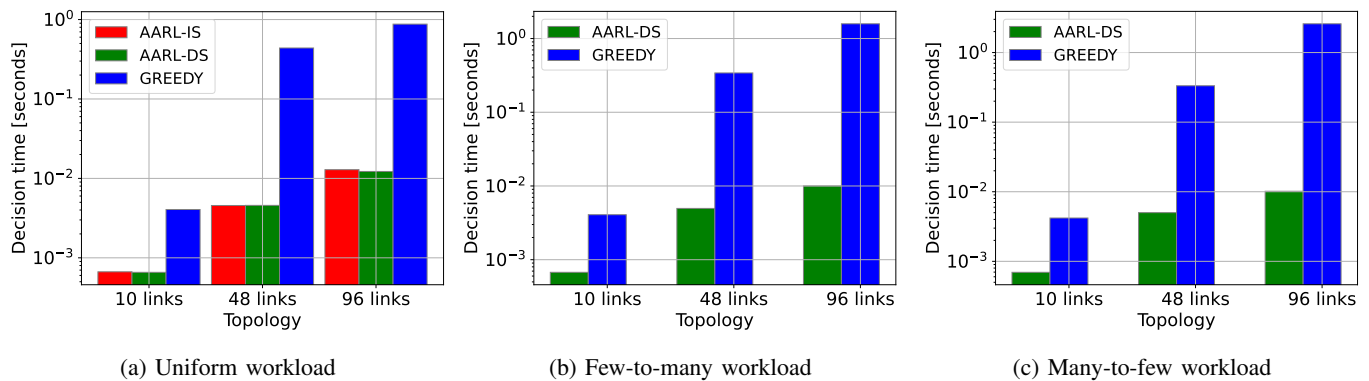


Fig. 13: The time it takes for AARL and GREEDY to make a scheduling decision (logarithmic scale)

| Workload - Algorithm | Topology | | |
|-----------------------|-----------------|------------------|-----------------|
| | Small (10-link) | Medium (48-link) | Large (96-link) |
| Uniform - GREEDY | 4.06 | 438.67 | 876.21 |
| Uniform - AARL-DS | 0.65 | 4.57 | 12.23 |
| Uniform - AARL-DI | 0.66 | 4.55 | 12.88 |
| Many-to-few - GREEDY | 4.07 | 341.41 | 1584.34 |
| Many-to-few - AARL-DS | 0.67 | 4.96 | 10.01 |
| Few-to-many - GREEDY | 4.19 | 333.13 | 2588.10 |
| Few-to-many - AARL-DS | 0.69 | 5 | 10.16 |

TABLE II: The time it takes to AARL and GREEDY to make a scheduling decision (in ms)

DRL algorithm that does not assume any prior knowledge of the interdependencies between different mmWave links. The proposed algorithm determines which subset of the mmWave links should be activated during each time slot and at what power level, and was demonstrated to work well for multiple workloads and topologies. It was shown to outperform the greedy algorithm both in terms of performance and running time, while meeting the timing constraints of 5G mmWave networks as specified by the ORAN model.

REFERENCES

- [1] A. Hakkarainen, J. Werner, M. Costa, K. Leppanen, and M. Valkama, "High-Efficiency Device Localization in 5G Ultra-Dense Networks: Prospects and Enabling Technologies," in *IEEE 82nd Vehicular Technology Conference*, New York, USA, 2015, pp. 1–5.
- [2] M. Mezzavilla, S. Dutta, M. Zhang, M. R. Akdeniz, and S. Rangan, "5G mmWave module for the ns-3 network simulator," in *Proceedings of the 18th ACM International Conference on Modeling, Analysis and Simulation of Wireless and Mobile Systems*. ACM, 2015, pp. 283–290.
- [3] Y. Niu, Y. Li, D. Jin, L. Su, and A. V. Vasilakos, "A survey of millimeter wave communications (mmWave) for 5G: opportunities and challenges," *Wireless networks*, vol. 21, no. 8, pp. 2657–2676, 2015.
- [4] atis, "atis3gpp specification," <https://www.atis.org/wp-content/uploads/3gpp-documents/Rel16/ATIS.3GPP.38.874.V1600.pdf>.
- [5] ORANA-IML, "Oran-wg2-aiml," <https://wiki.lfai.foundation/download/attachments/24281098/O-RAN.WG2.AIML-v01.02.02%20%282%29.docx?version=1&modificationDate=1609811670000&api=v2>.
- [6] ETSY, "Ts 138 300 v16.2.0," https://www.etsi.org/deliver/etsi_ts/138200_138299/138211/16.02.00_60/ts_138211v160200p.pdf.
- [7] T. Degris, P. M. Pilarski, and R. S. Sutton, "Model-free Reinforcement Learning with continuous action in practice," in *American Control Conference (ACC)*. IEEE, 2012, pp. 2177–2182.
- [8] F. Hu, *Opportunities in 5G networks: A research and development perspective*. CRC press, 2016.
- [9] A. Valadarsky, M. Schapira, D. Shahaf, and A. Tamar, "Learning to route with deep RL," in *NIPS Deep Reinforcement Learning Symposium*, 2017.
- [10] —, "A machine learning approach to routing," *arXiv preprint arXiv:1708.03074*, 2017.
- [11] Z. Xie, Y.-H. Huang, G.-Q. Fang, H. Ren, S.-Y. Fang, Y. Chen, and J. Hu, "Routenet: Routability prediction for mixed-size designs using convolutional neural network," in *IEEE/ACM International Conference on Computer-Aided Design (ICCAD)*. IEEE, 2018, pp. 1–8.
- [12] T. K. Vu, C.-F. Liu, M. Bennis, M. Debbah, and M. Latva-aho, "Path selection and rate allocation in self-backhauled mmWave networks," in *IEEE Wireless Communications and Networking Conference (WCNC)*, 2018, pp. 1–6.
- [13] S. Wang, H. Liu, P. H. Gomes, and B. Krishnamachari, "Deep Reinforcement Learning for dynamic multichannel access in wireless networks," *IEEE Transactions on Cognitive Communications and Networking*, vol. 4, no. 2, pp. 257–265, 2018.
- [14] M. G. Dogan, Y. H. Ezzeldin, C. Fragouli, and A. W. Bohannon, "A Reinforcement Learning Approach for Scheduling in mmWave Networks," in *MILCOM IEEE Military Communications Conference*, 2021, pp. 771–776.
- [15] A. HasanzadeZonuzi, D. Kalathil, and S. Shakkottai, "Reinforcement Learning for Multi-Hop Scheduling and Routing of Real-Time Flows," in *18th International Symposium on Modeling and Optimization in Mobile, Ad Hoc, and Wireless Networks (WiOPT)*, IEEE. IEEE, 2020, pp. 1–8.
- [16] S. Shen, T. Zhang, S. Mao, and G.-K. Chang, "DRL-Based Channel and Latency Aware Radio Resource Allocation for 5G Service-Oriented RoF-mmWave RAN," *Journal of Lightwave Technology*, vol. 39, no. 18, pp. 5706–5714, 2021.
- [17] S.-C. Tseng, Z.-W. Liu, Y.-C. Chou, and C.-W. Huang, "Radio Resource Scheduling for 5G NR via Deep Deterministic Policy Gradient," in *IEEE International Conference on Communications Workshops (ICC Workshops)*, 2019, pp. 1–6.
- [18] M. Feng and S. Mao, "Dealing with limited backhaul capacity in millimeter-wave systems: A deep Reinforcement Learning approach," *IEEE Communications Magazine*, vol. 57, no. 3, pp. 50–55, 2019.
- [19] J. Rischke, P. Sossalla, H. Salah, F. H. Fitzek, and M. Reisslein, "QR-SDN: Towards RL states, actions, and rewards for direct flow routing in software-defined networks," *IEEE Access*, vol. 8, pp. 174 773–174 791, 2020.
- [20] Z. Xu, J. Tang, J. Meng, W. Zhang, Y. Wang, C. H. Liu, and D. Yang, "Experience-driven networking: A deep Reinforcement Learning based approach," in *IEEE INFOCOM Conference on Computer Communications*, 2018, pp. 1871–1879.
- [21] Y. He, Z. Zhang, F. R. Yu, N. Zhao, H. Yin, V. C. Leung, and Y. Zhang, "Deep-Reinforcement-Learning-based optimization for cache-enabled opportunistic interference alignment wireless networks," *IEEE Transactions on Vehicular Technology*, vol. 66, no. 11, pp. 10433–10445, 2017.

- [22] W.-x. Liu, "Intelligent Routing based on Deep Reinforcement Learning in Software-Defined Data-Center Networks," in *Symposium on Computers and Communications (ISCC)*, 2019, pp. 1–6.
- [23] L. P. Kaelbling, M. L. Littman, and A. W. Moore, "Reinforcement learning: A survey," 1996.
- [24] Z. Mammeri, "Reinforcement Learning Based Routing in Networks: Review and Classification of Approaches," *IEEE Access*, vol. PP, pp. 1–1, 04 2019.
- [25] P. Sun, J. Li, J. Lan, Y. Hu, and X. Lu, "RNN Deep Reinforcement Learning for Routing Optimization," 12 2018, pp. 285–289.
- [26] A. Valadarsky, M. Schapira, D. Shahaf, and A. Tamar, "Learning to Route," in *Proceedings of the 16th ACM Workshop on Hot Topics in Networks*, ser. HotNets-XVI. New York, USA: Association for Computing Machinery, 2017, p. 185–191.
- [27] D. M. Casas-Velasco, O. M. C. Rendon, and N. L. S. da Fonseca, "DRSIR: A Deep Reinforcement Learning Approach for Routing in Software-Defined Networking," *IEEE Transactions on Network and Service Management*, vol. 1, no. 1, pp. 1–1, 2021.
- [28] J. Schulman, S. Levine, P. Moritz, M. I. Jordan, and P. Abbeel, "Trust region policy optimization," 2017.
- [29] J. Schulman, F. Wolski, P. Dhariwal, A. Radford, and O. Klimov, "Proximal policy optimization algorithms," 2017.
- [30] M. N. Islam, S. Subramanian, and A. Sampath, "Integrated access backhaul in millimeter wave networks," in *IEEE Wireless Communications and Networking Conference (WCNC)*, USA, 2017, pp. 1–6.
- [31] A. Lukowa, V. Venkatasubramanian, E. Visotsky, and M. Cudak, "On the coverage extension of 5G millimeter wave deployments using integrated access and backhaul," in *IEEE 31st Annual International Symposium on Personal, Indoor and Mobile Radio Communications*. USA: IEEE, 2020, pp. 1–7.
- [32] C. Saha, M. Afshang, and H. S. Dhillon, "Integrated mmWave Access and Backhaul in 5G: Bandwidth Partitioning and Downlink Analysis," in *IEEE International Conference on Communications (ICC)*, 2018, pp. 1–6.
- [33] C. Saha and H. S. Dhillon, "Millimeter wave integrated access and backhaul in 5G: Performance analysis and design insights," *IEEE Journal on Selected Areas in Communications*, vol. 37, no. 12, pp. 2669–2684, 2019.
- [34] B. Zhang, F. Devoti, and I. Filippini, "RL-based resource allocation in mmWave 5G IAB networks," in *Mediterranean Communication and Computer Networking Conference (MedComNet)*. IEEE, 2020, pp. 1–8.
- [35] M. Giordani, M. Mezzavilla, S. Rangan, and M. Zorzi, "Uplink-based framework for control plane applications in 5G mmWave cellular networks," *arXiv preprint arXiv:1610.04836*, 2016.
- [36] E. Gures, I. Shayea, A. Alhammadi, M. Ergen, and H. Mohamad, "A comprehensive survey on mobility management in 5G heterogeneous networks: Architectures, challenges and solutions," *IEEE Access*, vol. 8, pp. 195 883–195 913, 2020.
- [37] Y. Zhang, M. A. Kishk, and M.-S. Alouini, "A survey on integrated access and backhaul networks," *Frontiers in Communications and Networks*, vol. 2, p. 647284, 2021.
- [38] J. A. Shaw, "Radiometry and the Friis transmission equation," *American journal of physics*, vol. 81, no. 1, pp. 33–37, 2013.
- [39] L. Bonati, S. D'Oro, M. Polese, S. Basagni, and T. Melodia, "Intelligence and learning in O-RAN for data-driven NextG cellular networks," *IEEE Communications Magazine*, vol. 59, no. 10, pp. 21–27, 2021.
- [40] D. Johnson, D. Maas, and J. Van Der Merwe, "NexRAN: Closed-Loop RAN Slicing in powder - a Top-to-Bottom Open-Source Open-RAN Use Case," in *Proceedings of the 15th ACM Workshop on Wireless Network Testbeds, Experimental Evaluation Characterization*. New York, USA: Association for Computing Machinery, 2022.
- [41] M. Polese, L. Bonati, S. D'Oro, S. Basagni, and T. Melodia, "Understanding O-RAN: Architecture, Interfaces, Algorithms, Security, and Research Challenges," *arXiv preprint arXiv:2202.01032*, 2022.
- [42] O. Alliance, "O-RAN Working Group 2 AI/ML Workflow Description and Requirements," *ORAN-WG2. AIML v0102*, vol. 1, 2019.
- [43] A. Raffin, A. Hill, A. Gleave, A. Kanervisto, M. Ernestus, and N. Dormann, "Stable-Baselines3: Reliable Reinforcement Learning Implementations," *Journal of Machine Learning Research*, vol. 22, no. 268, pp. 1–8, 2021. [Online]. Available: <http://jmlr.org/papers/v22/20-1364.html>
- [44] C. Zhang, X. Ouyang, and P. Patras, "ZipNet-GAN: Inferring fine-grained mobile traffic patterns via a generative adversarial neural network," in *Proceedings of the 13th International Conference on emerging Networking Experiments and Technologies*, 2017, pp. 363–375.
- [45] C. Zhang, P. Patras, and H. Haddadi, "Deep Learning in Mobile and Wireless Networking: A Survey," *IEEE Communications Surveys Tutorials*, vol. 21, no. 3, pp. 2224–2287, 2019.
- [46] 3GPP, "Etsi ts 138 211 v16.2.0," 2020. [Online]. Available: https://www.etsi.org/deliver/etsi_ts/138200_138299/138211/16.02.00_60/
- [47] ETSI, "TS 123 501 - V15.10.0 - 5G; System architecture for the 5G System (5GS)," 2020. [Online]. Available: https://www.etsi.org/deliver/etsi_ts/123500_123599/123501/15.10.00_60/ts_123501v151000p.pdf

APPENDIX

In this appendix, we present the training statistics of the various AARL agents. Considers first Table A3, which shows the statistic for the 10-link topology. We can see that the time it takes for the various AARL agents to converge is approximately 7 hours of training time. For this topology, the batch size is 256 action/state/reward triples. The number of steps required for AARL to converge ranges between 1-2 million steps. The size of the hidden layers of the neural network is 256 neurons for each layer.

Table A4 presents the same statistics for the 48-link topology. We can see that the time it takes for the various AARL agents to converge is approximately 10 times longer than for the 10-link topology. Although the batch size for this topology was also 256 action/state/reward triples, the number of steps required for AARL to converge is much bigger: between 5.5-7 million steps. Each hidden layer of the neural network contains 1024 neurons.

In Table A5, for the 96-link topology, we see similar patterns with respect to training time and size of hidden layers. This time, the number of steps required to reach convergence was not significantly larger than for the 48-link topology, most likely due to a larger batch size that was used.

| Agent | Steps [M] | Batch Size | NN | Time [H] |
|-------------|-----------|------------|-----------|----------|
| 20-AARL-DI | 1.1 | 256 | [256,256] | 4 |
| 20-AARL-DS | 1.2 | 256 | [256,256] | 4 |
| 40-AARL-DI | 1.3 | 256 | [256,256] | 3 |
| 40-AARL-DS | 1.4 | 256 | [256,256] | 7 |
| 60-AARL-DI | 0.8 | 256 | [256,256] | 9 |
| 60-AARL-DS | 1.6 | 256 | [256,256] | 12 |
| 80-AARL-DI | 1.9 | 256 | [256,256] | 7 |
| 80-AARL-DS | 1.8 | 256 | [256,256] | 13 |
| 100-AARL-DI | 2 | 256 | [256,256] | 8 |
| 100-AARL-DS | 2.2 | 256 | [256,256] | 7 |

TABLE A3: Training statistics for the 10-link topology on a uniform workload of packets distribution.

| Agent | Steps [M] | Batch Size | NN | Time [H] |
|-------------|-----------|------------|-------------|----------|
| 20-AARL-DI | 7 | 256 | [1024,1024] | 45 |
| 20-AARL-DS | 6.15 | 256 | [1024,1024] | 43 |
| 40-AARL-DI | 7 | 256 | [1024,1024] | 27 |
| 40-AARL-DS | 5.85 | 256 | [1024,1024] | 38 |
| 60-AARL-DI | 5 | 256 | [1024,1024] | 39 |
| 60-AARL-DS | 7.25 | 256 | [1024,1024] | 44 |
| 80-AARL-DI | 5.85 | 256 | [1024,1024] | 41 |
| 80-AARL-DS | 6.5 | 256 | [1024,1024] | 44 |
| 100-AARL-DI | 6.15 | 256 | [1024,1024] | 36 |
| 100-AARL-DS | 9.2 | 256 | [1024,1024] | 74 |

TABLE A4: Training statistics for the 48-link topology on a uniform workload of packets distribution.

| Agent | Steps [M] | Batch Size | NN | Time [H] |
|-------------|-----------|------------|-------------|----------|
| 20-AARL-DI | 4 | 512 | [4096,4096] | 69 |
| 20-AARL-DS | 4.2 | 512 | [4096,4096] | 72 |
| 40-AARL-DI | 4.5 | 512 | [4096,4096] | 78 |
| 40-AARL-DS | 4.7 | 512 | [4096,4096] | 80 |
| 60-AARL-DI | 4.15 | 512 | [4096,4096] | 84 |
| 60-AARL-DS | 4.8 | 512 | [4096,4096] | 88 |
| 80-AARL-DI | 4.8 | 512 | [4096,4096] | 85 |
| 80-AARL-DS | 4.2 | 512 | [4096,4096] | 80 |
| 100-AARL-DI | 5 | 512 | [4096,4096] | 90 |
| 100-AARL-DS | 4.85 | 512 | [4096,4096] | 92 |

TABLE A5: Training statistics for the 96-link topology on a uniform workload of packets distribution.